ORNL/CSD/TM-39

Transport-Diffusion Comparisons for Small Core LMFBR Disruptive Accidents

E. T. Tomlinson

ORNL/CSD/TM-38
Distribution Categories
UC-79d, UC-79p

Contract No. W-7405 eng 26

COMPUTER SCIENCES DIVISION

TRANSPORT-DIFFUSION COMPARISONS FOR SMALL CORE LMFBR DISRUPTIVE ACCIDENTS*

E. T. Tomlinson

*Research sponsored by ORNL Neutron Physics Division

Date Published - November 1977

UNION CARBIDE CORPORATION, NUCLEAR DIVISION
operating the
Oak Ridge Gaseous Diffusion Plant • Oak Ridge National Laboratory
Oak Ridge Y-12 Plant • Paducah Gaseous Diffusion Plant
for the
DEPARTMENT OF ENERGY

CONTENTS

TRANSPORT-DIFFUSION COMPARISONS FOR SMALL CORE LMFBR DISRUPTIVE ACCIDENTS

E. T. Tomlinson

ABSTRACT

A number of numerical experiments were performed to assess the validity of diffusion theory for calculating the reactivity state of various small core LMFBR disrupted geometries. The disrupted configurations correspond, in general, to various configurations predicted by SAS3A for transient undercooling (TUC) and transient overpower (TOP) accidents for homogeneous cores and to the ZPPR-7 configurations for heterogeneous core. In all TUC cases diffusion theory was shown to be inadequate for the calculation of reactivity changes during core disassembly.

I. INTRODUCTION

The determination of situations for which diffusion theory is valid is one of the classic questions in reactor physics. There exists a certain class of problems for which diffusion theory is inapplicable, such as the calculation of the neutron flux in voids. These calculations can best be done by solving the neutron transport equation. There is, however, a range of problems for which it is difficult to a priori determine the validity of diffusion theory, such as partially disassembled homogeneous reactor cores and heterogeneous (parfait) reactor core designs.

The objective of this study is to examine the aforementioned situations and to determine where diffusion theory no longer yields acceptable results either directly, through the use of standard biasing techniques, or through the use of first-order perturbation theory. To

this end, the project was divided into two sections. The first section consists of an analysis of various snapshot models of a disrupted 330 MW(e) homogeneous liquid metal fast breeder reactor (LMFBR) core, using both diffusion and transport theory and perturbation theory. The models chosen were similiar to those predicted by the SAS3A[1] accident analysis core, but somewhat exaggerated. The large reactivity insertions predicted, would in reality not occur in an LMFBR core due to the effects of such phenomenon as Doppler broadening etc. The second section consists of an analysis of a 350 MW(e) heterogeneous core. The geometric configurations considered in this section were similar to those occurring in the Zero Power Plutonium Reactor (ZPPR-7)[2] experimental mock-up of the Clinch River Breeder Reactor Plant (CRBRP) alternate fuel management scheme (heterogeneous) core.

II. THE CROSS SECTIONS

A 7 group[3] macroscopic cross section library was created for use in the disrupted core neutronic analysis as well as for shutdown core physics studies. This library was collapsed from the 126 group psuedo composition-independent neutron library.[4] Prior to collapsing the cross sections the energy self-shielding effects in the macroscopic cross sections were accounted for by utilizing the homogeneous region Bonderanko treatment as it is coded into SPHINX.[5]

The XSDRNPM module of the AMPX[6] code system was used to collapse the fine group self shielded library to a 7 group P_3 library. The one-dimensional core model used for the calculation of the flux used in the collapse, is shown in Figure 1. The energy boundaries for the 7 group library are given in Table I.

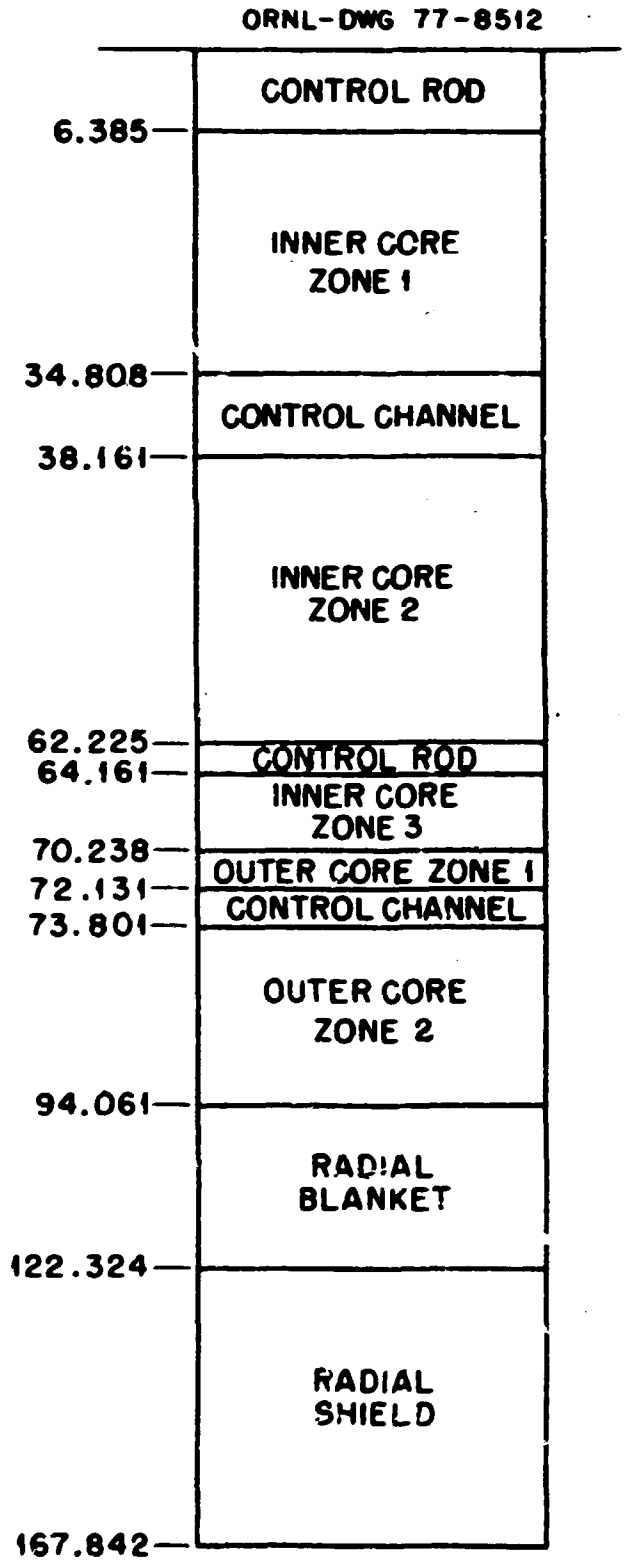

Fig. 1. The One-Dimensional Model of the CRBR Core Used For Cross Section Processing.

Table I. The Energy Boundaries for Seven Group Disrupted Core Cross Section Library

Group	Upper Energy Boundary (eV)
1	1.7333 + 07
2	8.1873 + 06
3	5.4881 + 06
4	2.4660 + 06
5	4.9787 + 05
6	1.2341 + 03
7	4.1399 - 01
	1.0000 - 05

A 7 group, transport corrected, P_0, macroscopic library was created for use in the diffusion calculations. The "inflow approximation" in the AXMIX[7] code was used for the calculation of the transport cross section.

Since these studies were scoping and comparative in nature, the cross sections were not reweighted for the heterogeneous core calculations, nor were the ZPPR-7 atom densities employed. Blanket and core materials that were generated for the homogeneous cases were merely interchanged.

III. THE CALCULATIONAL METHODS

A. Diffusion Theory

The diffusion calculations performed for this study were all done using the DOT3.5[8] discrete-ordinate code. Each calculation was considered to be converged when the fractional error in the k_{eff} eigenvalue was less than 1.0×10^{-4} and the point-wise error in the scalar flux was less than

1.0×10^{-4}. A typical calculation required 20-30 minutes of computing time on the IBM 360/91. Since DOT3.5 does not employ any convergence acceleration scheme on outer iterations and only non-sophisticated overrelaxation on the inner iterations, shorter computing times would be expected using codes such as VENTURE,[9] DIFF3D,[10] or FX2.[11] Central processor unit times for the "fine" mesh diffusion calculations were somewhat longer (approximately 90 min). The details of these cases are discussed later in this report.

B. Transport Theory

The first attempt to perform the transport calculations for this study was made using the DOT3.5 discrete ordinates code. Initial analysis indicated that the linear/step diamond difference[8] schemes in DOT3.5 could not be converged to the desired level. Model oscillations, i.e., cyclic switching between the linear and step models led to significant errors in the calculated k_{eff}'s and consequently in the reactivity changes. The point-wise angular fluxes could not be converged to less than 1.0×10^{-2} in some regions. As a result the decision was made to employ the newly developed DOT-4[12] discrete-ordinates code which has a "super-weighted" difference scheme that allows tighter convergence, see Appendix. The use of this difference scheme allowed the point-wise angular fluxes to be converged to a fractional deviation of less than 1.0×10^{-4} and the point-wise fission source to be converged to less than 1.0×10^{-3}.

The variations seen by switching differencing schemes were significant. The linear/step difference schemes calculated a sodium void worth for Case 1, described in the next section, of +0.318$ while the super-weighted

difference scheme calculated a worth of +0.034$. The accuracy of the super-weighted difference scheme was later compared to Monte Carlo calculations. The calculations used for this comparison are described later in this report. The discrete-ordinate calculation was in excellent agreement with the Monte Carlo calculation.

C. Perturbation Theory

Perturbation theory, particularly first-order perturbation in which the forward and adjoint fluxes at the unperturbed state are employed, has long been a method for estimating reactivity changes due to material changes in a reactor core. More recently "exact" perturbation theory, in which the adjoint at the perturbed state and the perturbed fission operator is used in the denominator of the perturbation equation, Eq (1), has been considered

$$\delta\rho = \langle \phi^*, (\delta F/k - \delta\Sigma + \delta S)\phi \rangle / \langle \phi^*, F\phi \rangle \qquad (1)$$

$\delta\rho$ = reactivity change

δF = change in the fission operator

$\delta\Sigma$ = change in the total cross section operator

δS = change in the scattering operator

k = unperturbed state eigenvalue

ϕ^* = unperturbed state adjoint flux (first order)
= perturbed state adjoint flux (exact)

ϕ = unperturbed state forward flux

$$F \begin{cases} = \text{unperturbed fission operator (first order)} \\ = F + \delta F = \text{perturbed fission operator (exact)} \end{cases}$$

The brackets in equation (1) indicate integration over all phase space. The perturbation results were calculated using a number of code modules[13-15] developed for use with the DOT series of codes. These modules allow the calculation of both first order and exact perturbation reactivity changes based on either transport or diffusion theory.

IV. THE HOMOGENEOUS CORE

The first section of this report deals with exaggerated hypothetical accident sequences similar to those that have been postulated for the 350 MW(e) homogeneous LMFBR core design.[16] Included in this section are the various disrupted configurations that were considered and the numerical results that were obtained.

A. Reactor Configurations

Five "snapshot" configurations were chosen for detailed neutronic analysis. Each configuration approximated, within the limits of R-Z geometry, a distinct phase in either the unprotected transient overpower (TOP) or transient undercooling (TUC) accident scenario. These configurations were defined as follows:

Case 1 — normal beginning of life (BOL) 350 MW(e) core,

Case 2 — initial sodium voiding phase of a TUC accident,

Case 3 — post-clad motion/pre-fuel motion phase of a TUC accident,

Case 4 – post-fuel motion/pre-shutdown phase of a TUC accident,

Case 5 – post-fuel motion phase of a TOP accident.

Case 1 – The Reference Core

The reference BOL core is depicted in Figure 2. The calculational model was extended through the shield in the radial direction (167.842 cm from the centerline) where a non-return boundary condition was imposed. The axial model extended from the non-return boundary at the lower edge of the lower attachment upward through the upper fission gas plenum, a distance of 367.436 cm to another non-return boundary. The interior mesh spacing and zone map are shown in Figure 3. A total of 3672 mesh points were used to describe this and all subsequent disrupted geometries.

An extra row of control rods was included in the model presented in Figure 2. This was done in an attempt to model the partially inserted control rods on the corners of the hex that approximate the inner core. The safety rods on the flats of this hex were parked in the upper axial blanket. This is a standard modeling technique employed by Westinghouse (W-ARD) fn modeling of the CRBRP.

Case 2 – The Sodium Void Model

The intent of the sodium void configuration was to model the initial phases of sodium voiding. In this configuration the sodium was voided from the high power to flow ratio channels, namely the center most subassemblies and the first row of subassemblies in the outer core. The voiding was assumed to occur in the active core region and to extend up through the upper axial blanket. The material changes and the zones

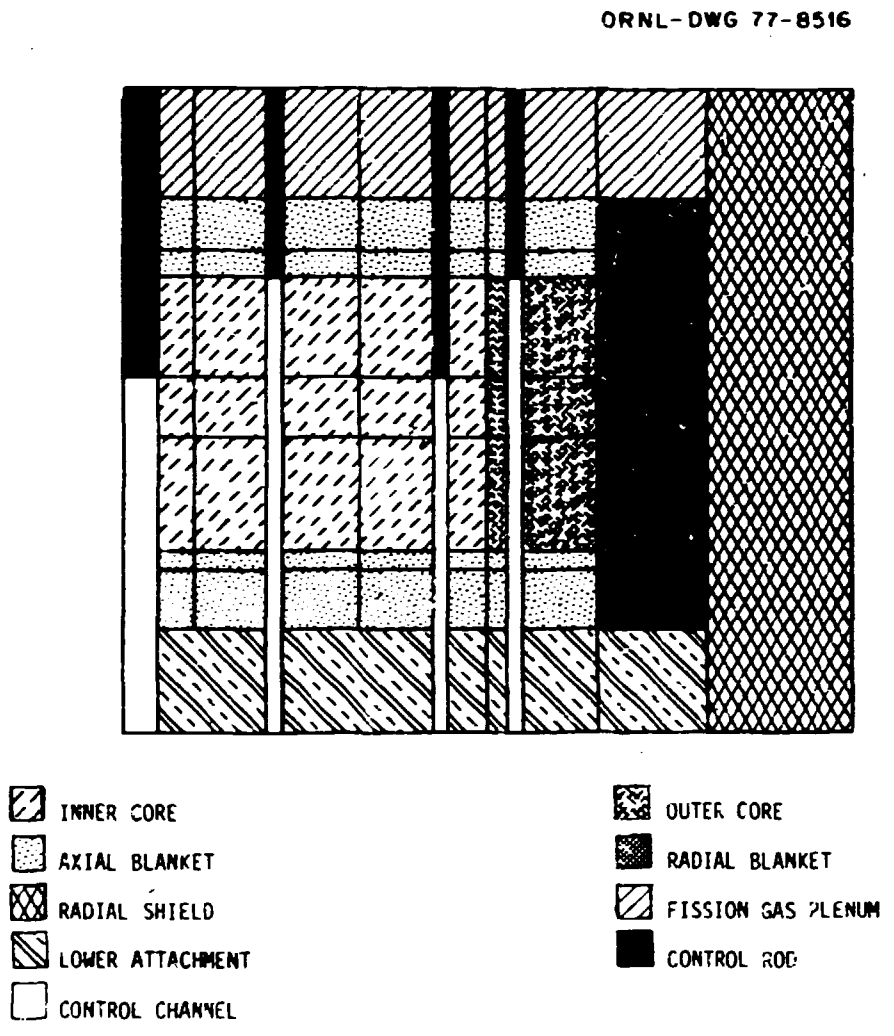

Fig. 2. Material Map for the Case 1 Disrupted Configuration.

involved in this perturbation are presented in Table II and illustrated in Figure 4.

Case 3 – The Post Clad Motion/Pre Fuel Motion Model

The third disrupted configuration is described in Table II and illustrated in Figure 5. This configuration was representative of the core after a large fraction, 78%, of the inner core has voided in addition to the first row of subassemblies in the outer core. The steel clad in the

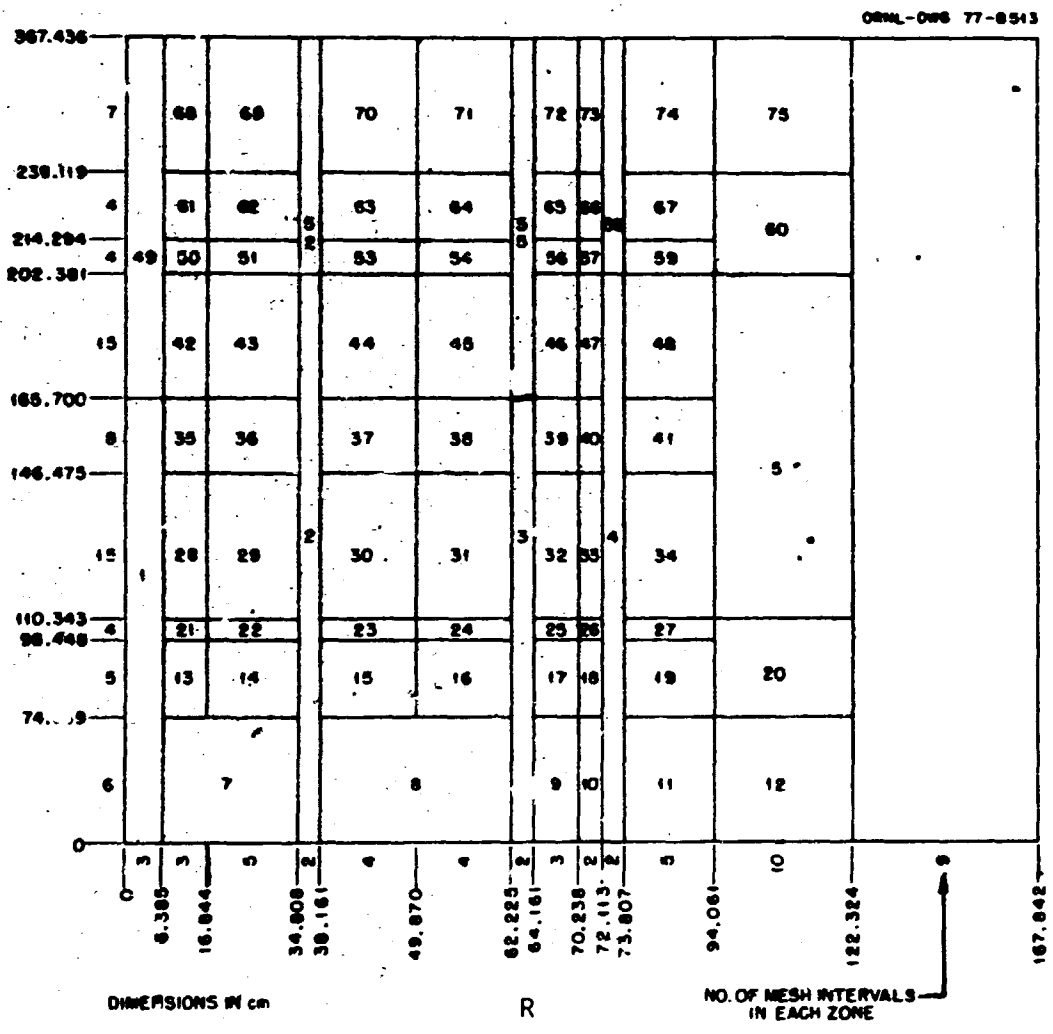

Fig. 3. Mesh Spacing and Zone Map for a 350 MW(e) LMFBR Core.

first three rows of subassemblies in the inner core and the first row of subassemblies in the outer core was assumed to have melted throughout the entire active core region. This material was then postulated to move upward and downward into the upper and lower axial blankets. Approximately 40% of the clad was assumed to freeze uniformly in the lower 11.913 cm of the upper axial blanket and 60% in the upper 11.895 cm of the lower axial blanket.

Table II. Disrupted Core Configurations

Problem ID	Effect of Interest	Quantity	Zones Involved*
Case 1	Reference		
Case 2	Sodium void	100% from	28,29,35,36,42,43,50,51 61,62 33,40,47,57,66
Case 3	Sodium void	100% from	21,22,23,26,28,29,30,31,33, 35,36,37,38,40 42,43,44,45,47,50,51,53,54, 57,61,62,63,64,66
	Move SS	100% from	28,29,30,35,36,37,42,43,44
		40% to	50,51,53
		60% to	21,22,23
	Move SS	100% from	33,40,47
		40% to	57
		60% to	26
Case 4	Same as 3 and Void Fuel	100% from	42,
		5% to	50,
		80% to	35
		10% to	28
		5% to	21
	Void Fuel	100% from	47
		5% to	57
		80% to	40
		10% to	33
		5% to	26
Case 5	Move Fuel	20% from	28,35,42
		20% to	61
		20% from	33,40,47
		20% to	66

*See Figure 3.

ORNL-DWG 77-8515

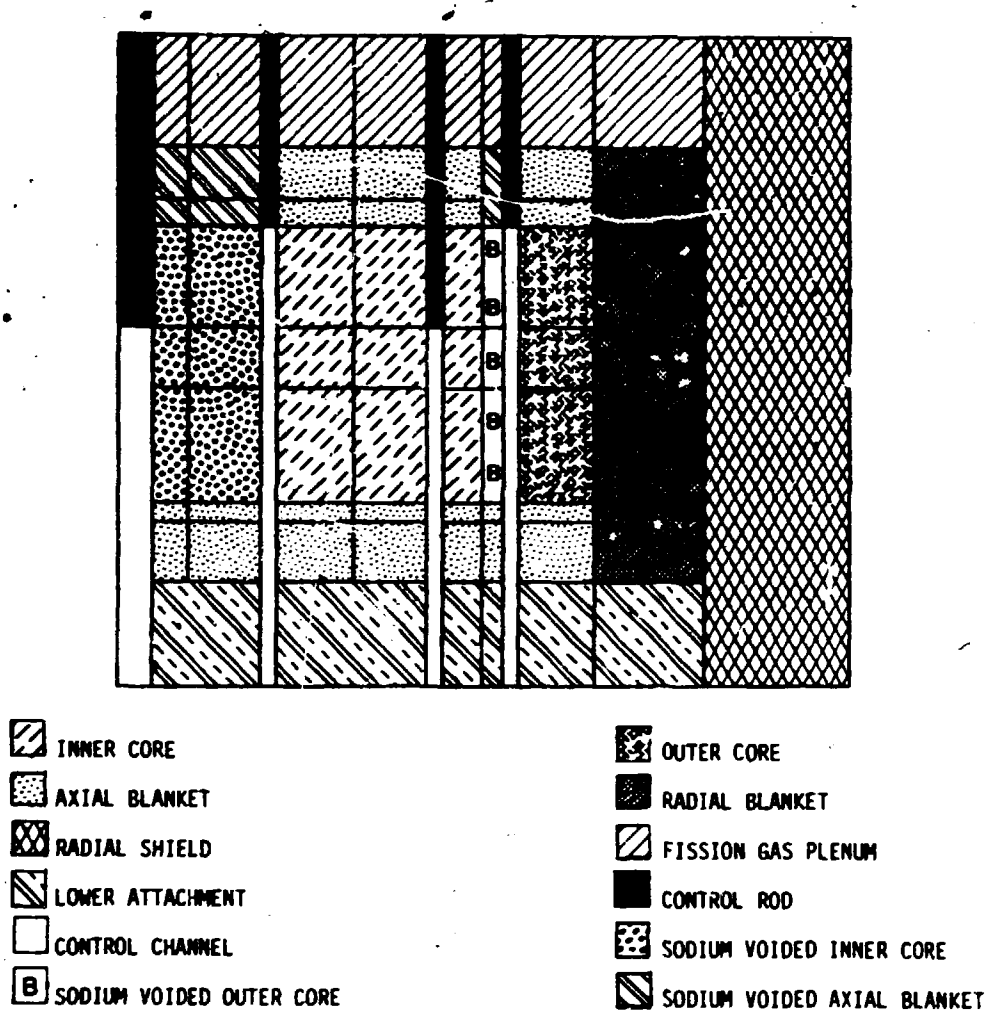

Fig. 4. Material Map for the Case 2 Disrupted Configuration.

Case 4 – The Post Fuel Motion/Pre Shutdown Model

The fourth disrupted configuration was described in detail in Table II and illustrated in Figure 6. This configuration was representative of a core shortly after the initiation of fuel slumping in the center six subassemblies of the inner core. The upper 36.681 cm of the unclad fuel

ORNL-DWG 77-8517

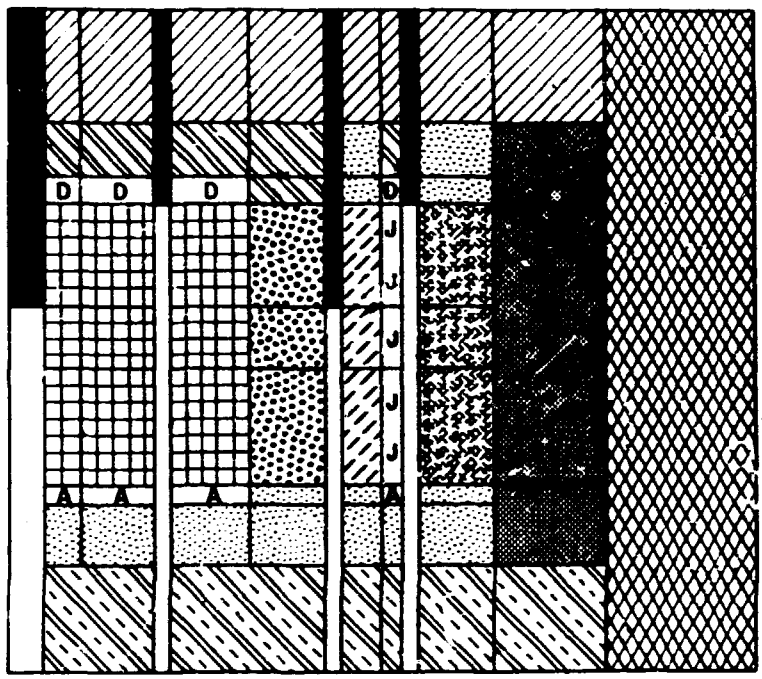

INNER CORE
AXIAL BLANKET
RADIAL SHIELD
LOWER ATTACHMENT
CONTROL CHANNEL
A 60% STEEL + AXIAL BLANKET
SODIUM AND STEEL VOIDED INNER CORE
D 40% STEEL + SODIUM VOID AXIAL BLANKET
OUTER CORE
RADIAL BLANKET
FISSION GAS PLENUM
CONTROL ROD
SODIUM VOIDED INNER CORE
SODIUM VOIDED AXIAL BLANKET
J SODIUM AND STEEL VOIDED OUTER CORE

Fig. 5. Material Map for the Case 3 Disrupted Configuration.

was assumed to redistribute itself uniformly in the lower portion of the subassembly, the lower axial blanket and the upper axial blanket. The majority of the fuel was assumed to slump under the force of gravity redistributing itself as follows: 80% in the center 19.225 cm of the

ORNL-DWG 77-8518

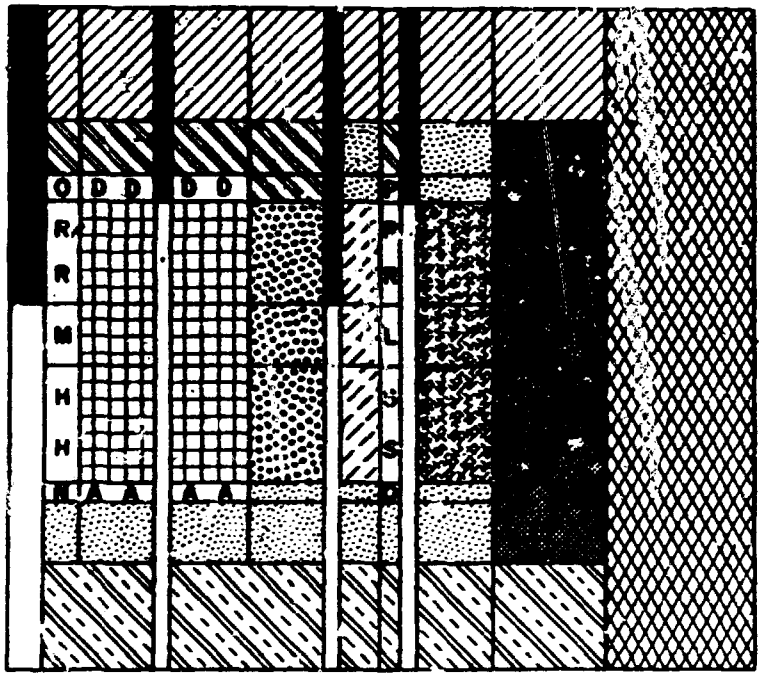

INNER CORE
AXIAL BLANKET
RADIAL SHIELD
LOWER ATTACHMENT
CONTROL CHANNEL
SODIUM AND STEEL VOIDED INNER CORE
D 40% CORE STEEL + SODIUM VOIDED AXIAL BLANKET
R VOID
H HIGH DENSITY INNER CORE FUEL
S HIGH DENSITY OUTER CORE FUEL
P 40% CORE STEEL + 5% OUTER CORE FUEL + SODIUM VOIDED AXIAL BLANKET
Q 60% CORE STEEL + 5% OUTER CORE FUEL + AXIAL BLANKET

OUTER CORE
RADIAL BLANKET
FISSION GAS PLENUM
CONTROL ROD
SODIUM VOIDED INNER CORE
SODIUM VOIDED AXIAL BLANKET
A 60% CORE STEEL + AXIAL BLANKET
M VERY HIGH DENSITY INNER CORE FUEL
L VERY HIGH DENSITY OUTER CORE FUEL
O 40% CORE STEEL + 5% INNER CORE FUEL + SODIUM VOIDED AXIAL BLANKET
N 60% CORE STEEL + 5% INNER CORE FUEL + AXIAL BLANKET

Fig. 6. Material Map for the Case 4 Disrupted Configuration.

active fuel region, 10% in the lower 36.132 cm of the active fuel region and 5% in the upper 11.895 cm of the lower axial blanket. The remaining 5% was postulated to move upward and freeze on or near the steel plug in lower 11.913 cm of the upper axial blanket.

Case 5 – The Post Fuel Motion Model

The fifth and final disrupted configuration was representative of the post TOP accident fuel relocation and is described in Table II and illustrated in Figure 7. It was postulated that 20% of the fuel was expelled from the fuel pins in the center subassemblies of the inner core and the first row of subassemblies in the outer core. It was then swept up and out of the core into the upper 23.825 cm of the upper axial blanket, where it was assumed to freeze. The steel clad and sodium in the axial blanket were assumed to remain in place.

These five particular disrupted configurations were chosen to be representative of the spectrum of material redistribution in severe core disruptive accidents. They by no means model all the possible nor necessarily the most reactive situations.

B. The Numerical Results and Analysis

Three discrete ordinate transport theory k_{eff} eigenvalue calculations (S_6P_3, S_4P_3, S_4P_0), were performed using various angular quadratures and scattering cross section expansions in order to access the effects of internal voids and anisotropic scattering. For all the cases examined no significant change was observed by varying the order of scattering

ORNL-DWG 77-8514

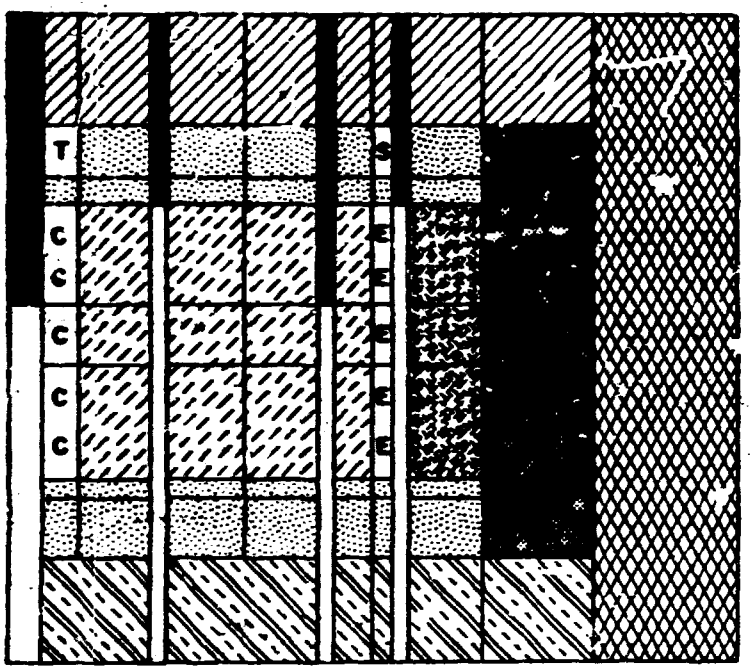

INNER CORE
AXIAL BLANKET
RADIAL SHIELD
LOWER ATTACHMENT
CONTROL CHANNEL
E LOW FUEL DENSITY OUTER CORE
S AXIAL BLANKET + OUTER CORE FUEL PLUG
OUTER CORE
RADIAL BLANKET
FISSION GAS PLENUM
CONTROL ROD
C LOW FUEL DENSITY INNER CORE
T AXIAL BLANKET + INNER CORE FUEL PLUG

Fig. 7. Material Map for the Case 5 Disrupted Configuration.

or the quadrature over the range cited above. A set of S_2P_0 calculations, not presented here, showed up to a 0.32% under prediction in k_{eff} when compared to the S_4P_0 results.

In order that the initial diffusion theory calculation proceed, a transport cross section of 1.0×10^{-4} was assumed for the voided regions in

Case 4. This led to an inordinately large diffusion coefficient which grossly overpredicted the neutron leakage from the core region into the axial blanket regions where neutrons were less important and consequently an underprediciton of k_{eff} resulted. Further diffusion calculations were performed to assess the effects of the assumed value of the diffusion coefficient on k_{eff}.

The dependence of k_{eff} on the value chosen for the diffusion coefficient in the internally voided regions is shown in Figure 8. The calculated multiplication factor is extremely sensitive to the choice of diffusion coefficients even though the voided region represented only 0.74% of the active core region. An investigation of the shape of the curve in Figure 8 revealed that for small values of the diffusion coefficient, D, the curve approximates the shape corresponding to Equation (1).

$$k \propto \frac{k^{\infty}}{1 + B^2 D/\Sigma a} \qquad (1)$$

where the terms have their standard definitions. As the value of the diffusion coefficient was increased the diffusion length, $\left(\frac{D}{\Sigma a}\right)^{1/2}$, also increased. Consequently, the spatial variation of the flux through the void in the axial direction became flat while the radial component remained virtually unchanged. This implied that the axial current, which was proportional to $\nabla\phi$, approached zero and therefore the axial DB^2 approached zero. As a result, Equation (1) became a constant which explains the flattening of the curve for large diffusion coefficients.

A more rational approach for changing a diffusion coefficient was based on the assumption that the transport mean free path can be approximated by the mean chord length of the voided region, Equation (2).

$$\bar{R} = \frac{4V}{S} \qquad (2)$$

where

V is the volume of the void and

S is the surface area of the void.

The multiplication factors calculated using this approach are shown in Figure [illegible]d in Table III. This approximation yielded good results compared to the expected value based on transport calculations (within 0.10% of the k_{eff} value needed to predict the same reactivity change as predicted by transport theory). Although the use of the mean chord length in the void resulted in a substantial improvement in the eigenvalue calculated using diffusion theory significant errors in the pointwise fluxes persisted.

Calculated k_{eff}'s

The k_{eff} eigenvalues calculated using discrete ordinate transport theory, diffusion theory, and Monte Carlo are presented in Table III. A comparison of the k_{eff}'s calculated using transport theory indicates that the effect of increasing either the number of angles in the quadrature or the order of scattering has little effect (<0.15%) on the results.

The adequacy of the mesh was examined by comparing the k_{eff}'s calculated with the Monte Carlo code KENO[17] with their corresponding DOT 4 values.

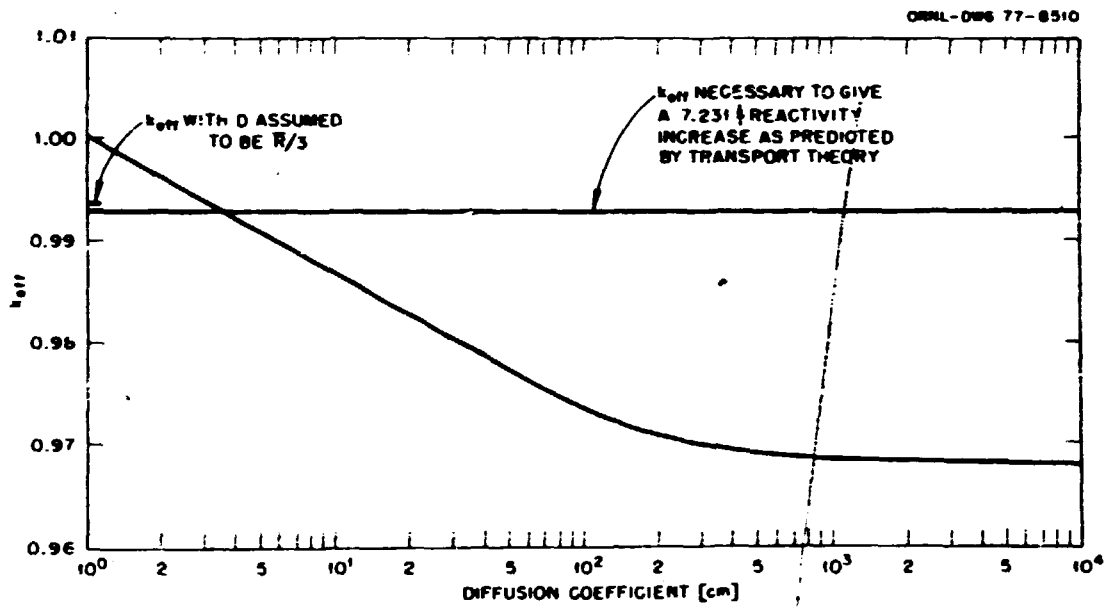

Fig. 8. The Dependence of the Calculated k_{eff} vs the Choice of Void Diffusion Coefficients.

Table III. Calculated k_{eff} for the Various Disrupted Core Configurations

	Super-Weighted		Linear/Step	Super-Weighted	Coarse Mesh[1] Diffusion	Fine Mesh[2] Diffusion	Keno P_8
	S_4P_3	S_4P_3	S_4P_3	S_4P_8			
Case 1	0.985797	0.985950	0.98529	0.987033	0.970650	0.967040	0.98390 ± 0.00255
Case 2	0.985893	0.986057	0.98628	0.987215	0.969881		
Case 3	1.00017	1.00053		1.00165	0.979977		
Case 4	1.00881	1.00915	1.00877	1.01036	0.993463[3] 0.968476[4]	0.989108[3] 0.963693[4]	1.00529 ± 0.00293
Case 5	0.979032	0.979203		0.980218	0.963420		

[1] 54 × 68 mesh.

[2] 108 × 136 mesh.

[3] D = R/3 cm

[4] D = 3333.33 cm

in void

This was done only for the most severely disrupted (most heterogeneous) configuration since this was where inadequacies in the mesh would most likely have occured. The DOT-4 results were in excellent agreement with the Monte Carlo results (within 2σ) thus providing a degree of confidence in the mesh used in the transport calculations. The linear/step model calculations are presented here for completeness only and will not be considered further for reasons discussed in Section III of this report.

Further examination of Table III indicated that diffusion theory consistently underpredicted k_{eff} from 1.62% for Case 5, to 2.06% for Case 3. Compared to transport theory, there was a 1.5% underprediction of k_{eff} for the reference Case 1. The results for Case 4 were purposely deleted from this comparison because of the arbitrary choice of diffusion coefficients in the voided regions. The percent underprediction in k_{eff} could have been much larger if these results were included.

A "fine mesh" diffusion calculation was performed on both the Case 1 and Case 4 disrupted configurations. The fine mesh was defined by uniformly doubling the original mesh. Diffusion coefficients of 3333.33 and $\bar{R}/3$ were assumed for the in-core voids. Based on these cases there did not appear to be any significant advantage in using the fine mesh for the diffusion calculations and the remainder of the configurations were calculated using "coarse mesh" diffusion theory.

Diffusion theory's continuous underprediction of k_{eff} was caused by an overprediction of the neutron leakage from the active core zone. The neutron leakage out of the core at the upper core/axial blanket interface near the core center was calculated to be approximately 15% higher in a diffusion theory than calculation in an equivalent transport calculation

for the reference core. The magnitude of this discrepancy increased as the density of the core zone decreased (i.e. the diffusion coefficient increased). Consequently, no single bias factor could a priori be derived which, when applied to the diffusion theory results, would yield equivalent transport results.

Reactivity Changes

Behavior similiar to that observed for the multiplication factors was observed for the calculated reactivity changes between configurations, Table IV. These reactivity changes were calculated using the direct k difference techniques.

Table IV. Calculated Reactivity Changes for the Various Disrupted Configurations

$\delta\rho$[\$]

	Super-Weighted		Linear/Step	Super-Weighted	Coarse Mesh[1] Diffusion	Fine Mesh[2] Diffusion	Keno P_0
	S_4P_3	S_4P_3	S_4P_3	S_4P_0			
Case 2	0.031	0.034	0.318	0.058	−0.256		
Case 3	4.556	4.619		4.620	3.064		
Case 4	7.231	7.287	7.382	7.310	7.393[3] −0.723[4]	7.210[3] −1.131[4]	6.758 ± 1.224
Case 5	−2.190	−2.184		−2.201	−2.416		

β_{eff} = 0.0032

[1] 54 × 68 mesh

[2] 108 × 136 mesh

[3] D = R/3 cm

[4] D = 3333.33 cm

} in void

The reactivity changes calculated using transport theory were all in excellent agreement with each other (within a few cents) indicating that neutron streaming and anisotropic scattering could be accounted for in these models by using low order transport methods such as S_4P_0. The S_2P_0 results underpredict the reactivity change by as much as 0.44\$. The discrete ordinate results lie within 1 σ of the Monte Carlo calculated reactivity change, which gave an air of confidence to the results.

A closer comparison of the diffusion and transport results revealed that the underprediction of $\delta\rho$ ranged from 0.22\$ for Case 2 to 1.55\$ for Case 3. Again Case 4 was not considered because of the uncertainties in the calculated reactivity changes for the arbitrary choice of diffusion coefficients.

Since perturbation theory is a standard procedure for determining material worths for safety calculation the validity and accuracy of a number of perturbation techniques were investigated. Both transport and diffusion theory perturbation methods were used to calculate the reactivity changes between cases.

The transport perturbation calculations were performed using the S_4P_3 forward and adjoint fluxes because S_4 and S_6 results were of comparable accuracy and S_4 calculations were less costly to compute. First order and exact perturbation calculations were performed for each of the four disrupted configurations. The results of these calculations are presented in Table V.

First-order transport perturbation continuously overpredicted the magnitude of the reactivity change, for both positive and negative changes. This overprediction was conservative for positive reactivity changes, but

Table V. Reactivity Changes Calculated Using Transport Perturbation Theory

$\delta\rho$[$]

	Direct	First-Order Perturbation	Exact Perturbation
Case 2	0.034	0.193	-0.044
Case 3	4.619	5.512	4.304
Case 4	7.287	9.150	6.970
Case 5	-2.184	-2.316	-2.321

not for negative reactivity changes (i.e., the system was calculated to be further subcritical than it actually was). The use of exact perturbation theory yielded reactivity changes that were within a few percent of the direct k_{eff} difference calculations. The difficulty with the use of exact perturbation theory was that the perturbed adjoint must be calculated for each disrupted configuration (a priori knowledge of the final configurations).

First-order diffusion perturbation theory fairs less well than the first-order transport perturbation theory as can be seen in Table VI. The discrepancy for some cases was as large as a factor of 5 for the magnitude of the change and in Case 2 even the sign of the reactivity change was incorrect. Again, exact diffusion perturbation theory could be used to calculate reactivity changes that were in good agreement with the direct diffusion k_{eff} difference results, but still not in agreement with direct transport results.

A closer examination of the first-order versus exact perturbation theory is presented in Table VII. The largest discrepancy was in the

Table VI. Reactivity Changes Calculated Using Diffusion Perturbation

$\delta\rho$[$]

	Direct	First Order Perturbation	Exact Perturbation
Case 2	-0.256	-0.743	-0.231
Case 3	3.064	-1.587	3.189
Case 4	7.393	1.458	7.495
Case 5	-2.416	-2.439	-2.420

Table VII. Relative Error in Reactivity Contributions Based on Diffusion Perturbation Theory [% $\delta\rho$($)]*

	Case 2	Case 3	Case 4	Case 5
Diffusion	23.48	29.48	43.67	3.99
Removal	0.58	-0.52	2.12	0.97
Scatter	1.49	1.70	4.68	1.09
Fission	0.00	0.00	-0.51	0.72

* % $\delta\rho$($) = (FOP-EXACT)/EXACT * 100

calculation worth of the diffusion coefficient, up to a 43% error. The largest error occurred in the case in which a large amount of core material had been moved and the shape of the adjoint had drastically changed.

An examination of the diffusion theory first order perturbation results revealed that the net contribution of the removal and scattering terms, was near zero, leaving difference between the diffusion and fission terms to determine the final reactivity change. Therefore the large errors in the leakage worths were the dominant contributors to discrepancies in

the total calculated reactivity change. It should be noted here that the leakage (diffusion) is implicitly calculated in the transport perturbation and thusly does not contribute explicitly to errors in the calculated reactivity change. It is for this reason that first-order transport perturbation tends to yield reactivity changes that are in better agreement with the direct k_{eff} difference and exact perturbation results.

In view of the implicit nature of the leakage worth calculation in transport calculations, a hybrid diffusion/transport P_1 perturbation technique[18] was investigated. This method involved the calculation of the partial currents for each interval from the diffusion theory scalar fluxes. These partial currents were then treated as the components of the first flux moment and folded with the P_1 scattering cross section. The remainder of the calculation proceeded as a normal transport perturbation calculation thus accounting for the leakage implicitly.

This hybrid method was applied to each case using both the first-order and exact perturbation approximations. The results of these calculations are presented in Table VIII. The first-order P_1 perturbation results were significantly improved over the first-order diffusion theory perturbation results. In fact they were in excellent agreement with the first-order transport perturbation results. This indicated that this hybrid diffusion/transport P_1 technique may be used to yield transport perturbation results with diffusion theory computing expense. The P_1 method by no means calculates the correct (direct k_{eff} difference) reactivity changes, but it does provide a substantial degree of improvement over standard first-order diffusion theory perturbation. No substantial improvement was noted for exact perturbation theory.

Table VIII. Reactivity Changes Calculated Using Diffusion Theory Fluxes and Currents in a Transport Perturbation Calculation

	Direct Transport	First-Order			Exact		
		Diffusion	Transport	P_1	Diffusion	Transport	P_1
Case 2	0.034	-0.743	0.193	0.151	-0.231	-0.044	-0.216
Case 3	4.619	-1.587	5.512	5.549	3.189	4.304	3.261
Case 4	7.287	1.458	9.150	9.139	7.495	6.970	6.539
Case 5	-2.184	-2.439	-2.316	-2.412	-2.420	-2.321	-2.420

V. THE HETEROGENEOUS CORE

The second phase of this study deals with a few preliminary calculations of sodium void worth based on the ZPPR-7 mock-up of a 350 MW(e) heterogeneous "parfait" core design. Since these were preliminary scoping studies, the macroscopic cross sections for the homogeneous core were used for these calculations. Included in this section are the various voided configurations that were studied and the numerical results that were obtained.

A. Reactor Configurations

Three "snapshot" configurations representing various phases of the ZPPR-7 sodium voiding experiment were chosen for this study. The configurations considered were as follows:

Case 1 – Reference unperturbed assembly,

Case 2 – Sodium voided in the driver zones,

Case 3 – Sodium voided in the central blanket zone.

The square drawered ZPR matrix assembly was modeled in R-Z geometry as suggested in reference 2.

Case 1 – The Reference Assembly

The reference assembly is depicted in Figure 9. The calculational model was extended through the radial shield (147.253 cm from the centerline) where a non return boundary condition was imposed. Since all material movements in the ZPPR-7 assembly were assumed to be symmetric with respect to the core midplane, only the upper half-core was modeled in the axial direction. The axial model extends from the core midplane through the upper axial shield-reflector (104.806 cm from the assembly midplane). A symmetric boundary condition was applied at the midplane and non-return boundary condition was imposed at the upper edge of the axial shield-reflector. The interior mesh spacing and zone map are illustrated in Figure 10. A total of 1711 mesh points was used to describe this and all the subsequent geometries. It should be noted that the R-Z models presented here are very crude and by no means are representative of the real situation.

Case 2 – The Voided Driver Model

The intent of the sodium voided driver configuration was to model a sodium void that extends 30.48 cm above and below the assembly midplane in the inner two high-power to flow ratio driver zones. This configuration is described in Table IX and depicted in Figure 11.

ORNL-DWG 77-8519

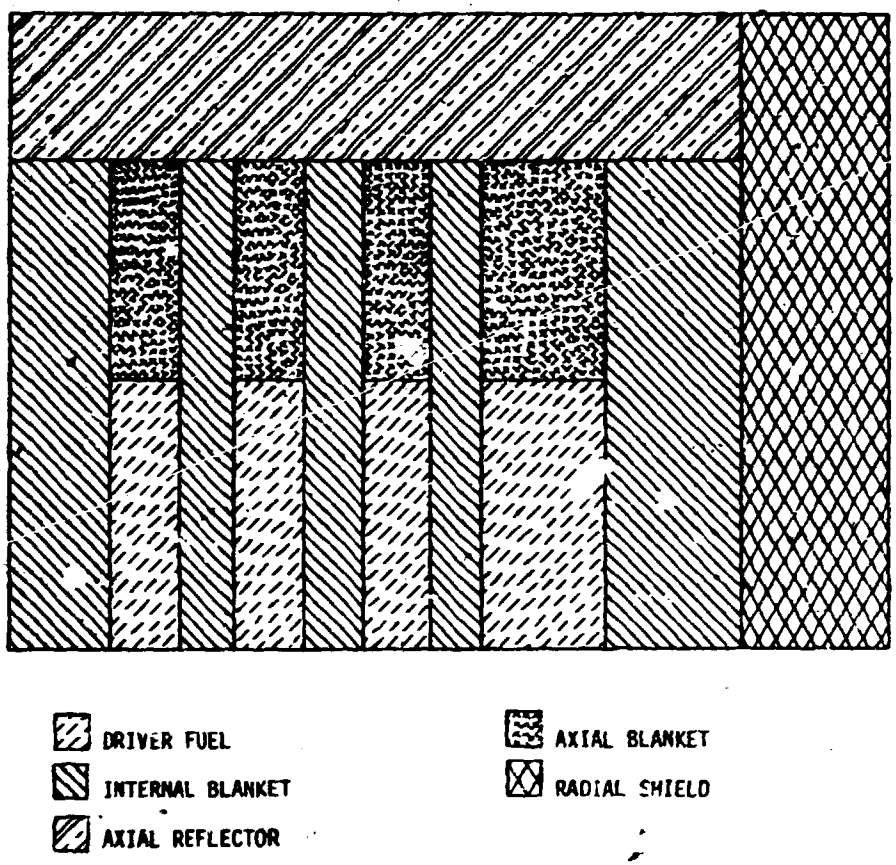

Fig. 9. Material Map for the Case 1 Disrupted Configuration in ZPPR-7.

Case 3 — The Voided Blanket Model

In this configuration sodium has been symmetrically removed about the assembly midplane in the central blanket region. The voiding was assumed to extend from 30.48 cm below the midplane to 30.48 cm above the midplane. This configuration is also described in Table IX. and depicted in Figure 12.

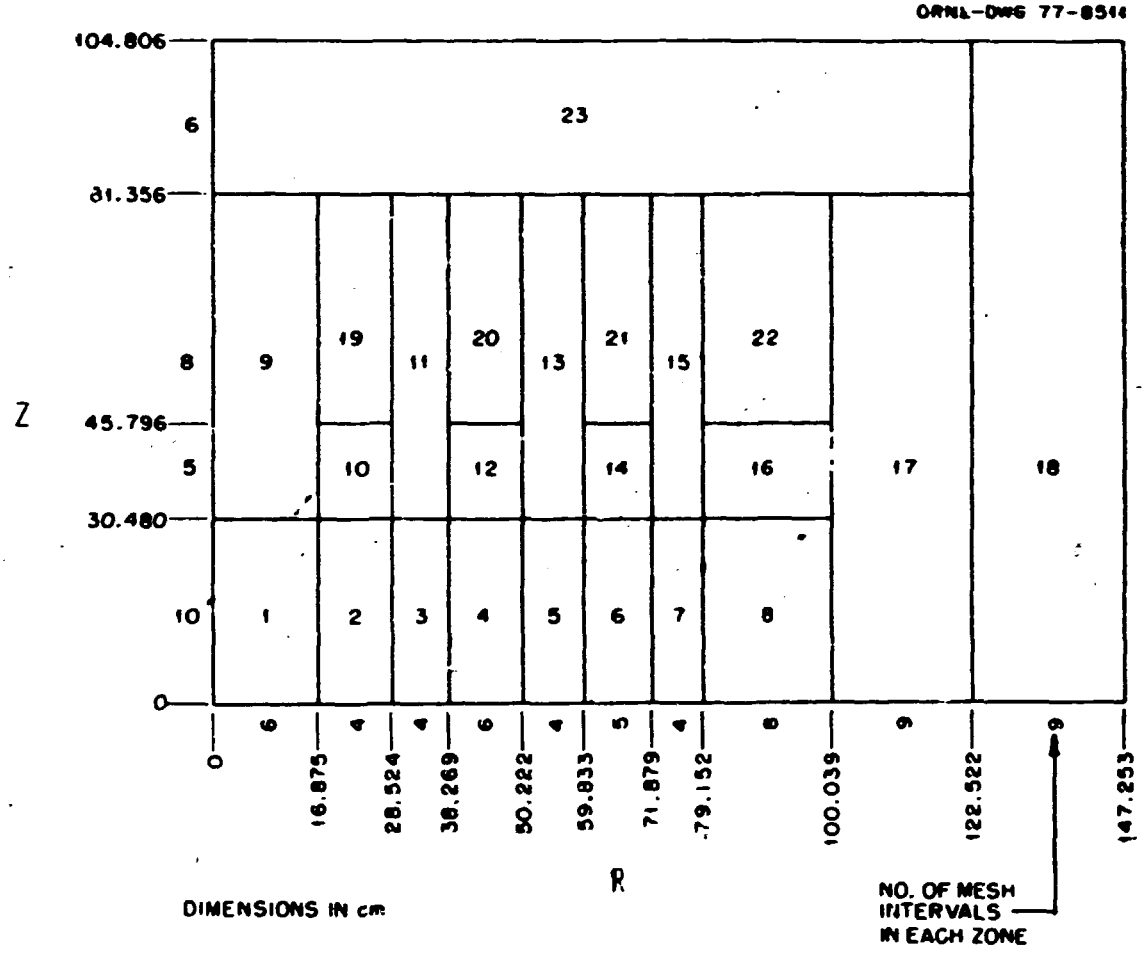

Fig. 10. Mesh Spacing and Zone Map for ZPRR-7.

Table IX. Problem Definition for ZPPR-7

Problem ID	Effect of Interest	Quantity	Zones Involved*
Case 1	Reference		
Case 2	Sodium Void	100%	2,4
Case 3	Sodium Void	100%	1

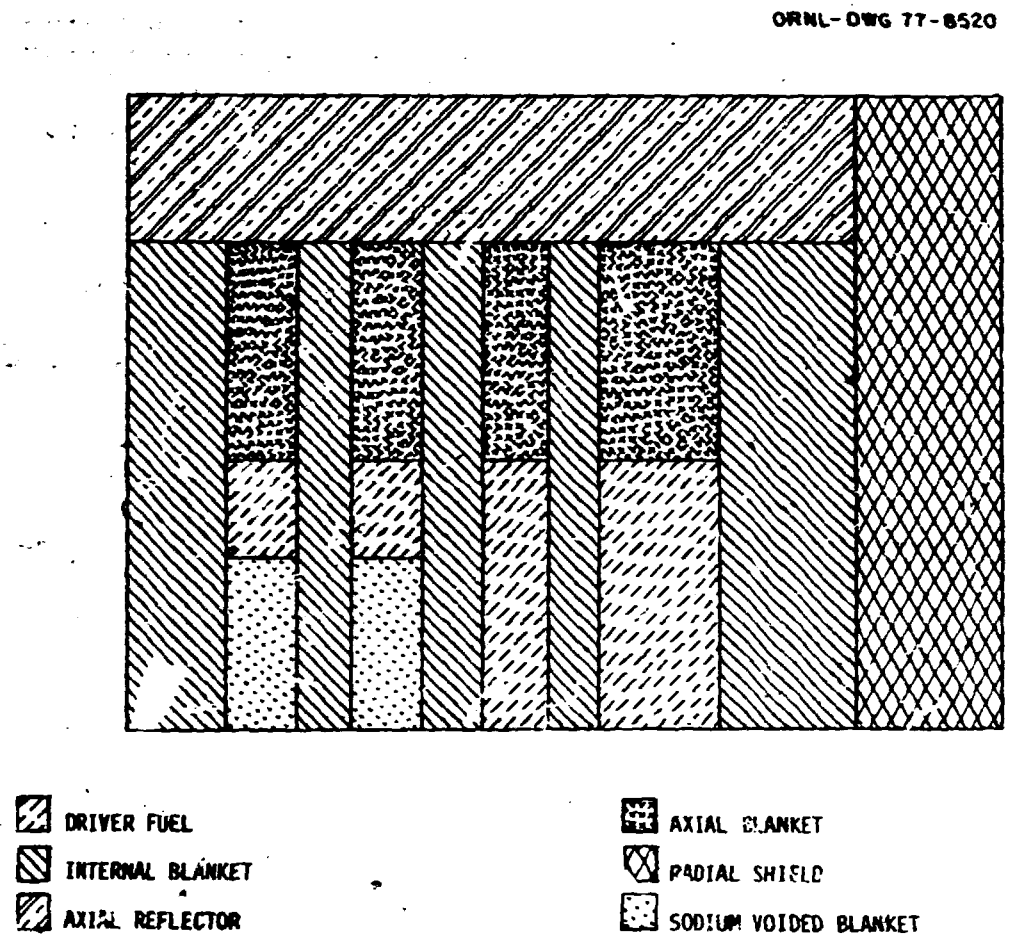

Fig. 11. Material Map for the Case 2 Disrupted Configuration in ZPPR-7.

B. Numerical Results and Analyses

As stated previously, the purpose of this section is not to analyze ZPPR-7, but to provide a first-pass transport/diffusion methods comparison based on various configurations used in ZPPR-7. The results presented here should be viewed in that context.

The calculated k_{eff} for the various configurations studied are presented in Table X. Diffusion theory underpredicted k_{eff} by 0.61 for the reference case. Differences of the same magnitude were calculated for the two disrupted cases. This does not necessarily mean that

ORNL-DWG 77-8521

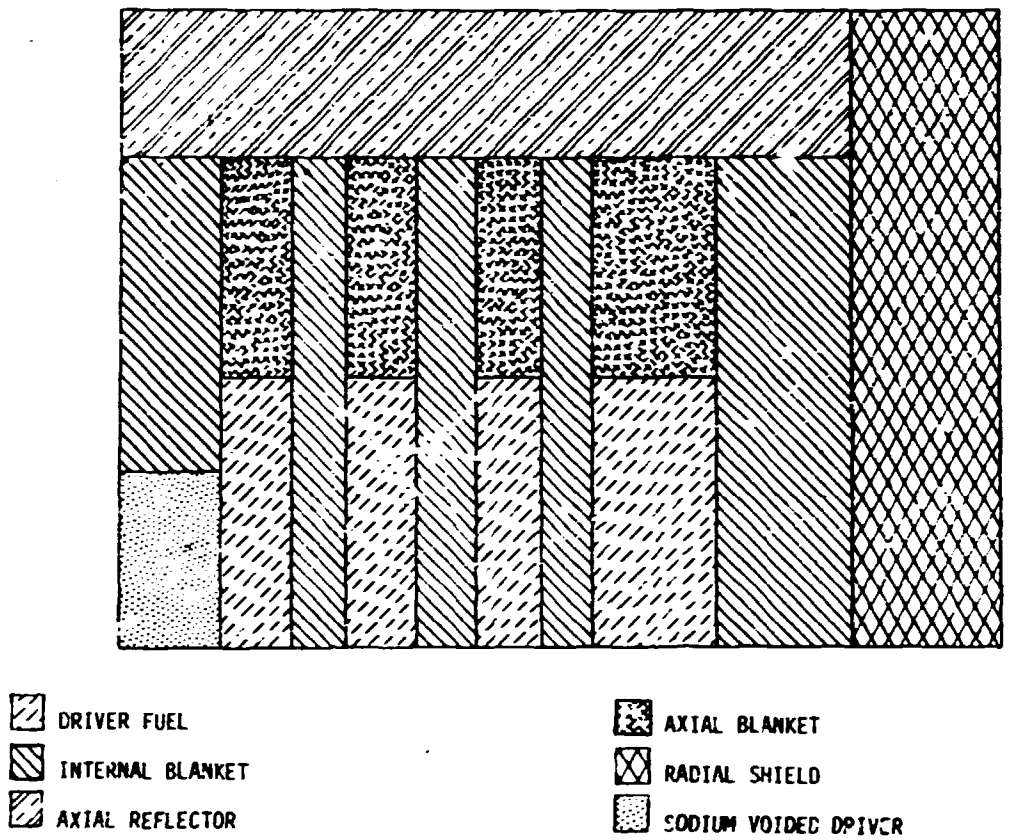

Fig. 12. Material Map for the Case 3 Disrupted Configuration in ZPPR-7.

Table X. Calculated k_{eff} for the Various Disrupted Heterogeneous Core Configurations

	S_4P_3	Diffusion
Case 1	0.954826	0.948648
Case 2	0.957407	0.950956
Case 3	0.955053	0.948841

a single bias factor can be applied to the diffusion results to obtain the transport results for more disrupted configurations because only small perturbations to the system's geometry were considered. Large movements of core material could reveal greater transport/diffusion discrepancies; however, for the specific cases addressed in this study a constant bias factor did exist.

Prior to discussing the disrupted core results in depth, four points concerning the reference core calculations are of interest and are presented here.

- In all the fertile (blanket) regions, diffusion theory consistently gave a harder spectrum than transport theory.
- In all fissile (driver) regions, diffusion theory consistently gave a softer spectrum than transport theory.
- The total flux was depressed more in the fertile regions for the transport calculation than for the diffusion calculation.
- The U-238 capture rate followed the same trends as the total flux.

The direct k_{eff} difference reactivity changes for the two disrupted cases are presented in Table XI. As in the homogeneous case, diffusion theory predicted the assembly to be in a less reactive state than that predicted by transport theory. There was a 10% underprediction of the reactivity change in the voided driver calculation and a 14% underprediction in the voided blanket configuration. The effects of this discrepancy are illustrated in Table XII. The C/E values calculated using diffusion theory taken from reference 2 and the T/D, transport/diffusion ratios, were taken from this report. The inclusion of the

Table XI. Calculated Reactivity Changes for the Various Disrupted Heterogeneous Core Configurations $\delta\rho(\$)$

	S_4P_3	Diffusion
Case 2	0.882	0.799
Case 3	0.078	0.067

$\beta_{eff} \equiv 0.0032$

Table XII. Transport Corrected C/E for ZPPR-7.

	C/E[a]	T/D[b]	C/E[c]
Case 2	0.865	1.104	0.955
Case 3	0.930	1.164	1.083

[a] C/E values calculated using diffusion theory,
[b] see reference 2.
$\delta\rho$Transport/$\delta\rho$Diffusion.
[c] Transport adjusted C/E. (C/E X T/D)

transport effects tends to alleviate a large fraction of the calculational disagreement with the experiment. It should be kept in mind, however, that these results only indicate trends since the atom densities and cross section treatments used for the heterogeneous core studies were not rigorous.

VI. CONCLUSIONS

The overriding conclusion of this study was that for all cases investigated diffusion theory and first-order diffusion perturbation theory were inadequate for the calculation of the reactivity state of severely disrupted homogeneous LMFBR cores. There appears to be no

single bias factor that can a priori be calculated and applied to the calculated multiplication factor to obtain equivalent transport theory results. Similarly there are no single bias factors existing that can be applied to the reactivity changes calculated using diffusion theory or diffusion perturbation theory to obtain equivalent transport theory results.

When compared to transport theory, diffusion theory also underpredicted k_{eff} for heterogeneous, parfait, core calculations. A single bias factor did exist that would be applied to the diffusion theory results to obtain transport results for the situation in which various parts of the core were voided of sodium. This does not necessarily mean that a single bias factor could be a priori calculated and applied to diffusion results to obtain transport results for severe core disruptions. The sodium voiding cases represented relatively small perturbations to the system with minimal material motion. Large movements of core material could reveal greater transport/diffusion discrepancies. This is presently being investigated.

The major failing of diffusion theory was in its consistent overprediction of leakage from zones of low density. This effect was particularly evident in the first order diffusion perturbation results where errors as large as 43% in the calculation of leakage (diffusion coefficient) worths existed. First order transport perturbation theory, where the leakage terms are accounted for implicitly gave results that were in better agreement with direct k_{eff} difference calculations, however, the calculated change in reactivity (both positive and negative) was consistently overpredicted. For negative insertions this was a nonconservative approximation.

A number of other investigators at other installations have also performed calculations similar to those carried out in this study. Recently, Cahalan at Argonne National Laboratory performed a number of numerical experiments[19] and obtained results that agree both qualitatively and quantitatively with the results of this study. His results support the results presented here in that transport effects, especially, in the calculation of neutron leakage from low density regions must be included in fast reactor safety neutronics. He has investigated a method that incorporates transport calculated leakages in diffusion theory calculations and has shown that this method gave significantly improved diffusion theory results. Also at ANL, work is under way to investigate the applicability of directional-dependent diffusion coefficients[20] to remedy the failure of classic diffusion theory to correctly calculate neutron leakage.

During the course of this study a hybrid transport/diffusion perturbation theory was developed. The P_1 perturbation method offers first order transport perturbation theory accuracy with diffusion theory computation times. This hybrid calculation while not being a solution to all the safety related neutronic problems does provide a means of improved accuracy at low computational costs.

It is not clear, however, which approach should be taken, whether the diffusion theory approximations should be eliminated completely and a low order transport (S_4P_0) method be perfected for fast reactor safety related neutronics calculations, or a hybrid diffusion/transport methods such as Cahalan's in conjunction with a hybrid perturbation method such as the method presented in this study should be pursued for improving fast reactor safety neutronics calculations. The low order transport method would be

preferable as it has the potential of handling more severe streaming and anisotropy effects where diffusion theory and hybrid P_1 theory are limited in their ability to calculate these effects.

VII. ACKNOWLEDGMENTS

The author would like to acknowledge the efforts of P. B. Fox in obtaining the Monte Carlo results presented in this report and also W. A. Rhoades and W. W. Engle, Jr., for the discussion of the "super-weighted" differencing scheme that is presented in the appendix. The author would also like to thank R. L. Childs for many discussions concerning the P_1 perturbation technique. The efforts of C. P. Trammell and B. O. Neeley in typing this manuscript are greatly appreciated.

VIII. REFERENCES

1. W. R. Bohl, et al., *An Analysis of Transient Undercooling and Transient Overpower Accidents without Scram on the Clinch River Breeder Reactor*, ANL/RAS 75-29, Argonne National Laboratory (July 1975).
2. *Twentieth Quarterly Report: Critical Experiments and Analysis, July-September 1976*, GEAP-13771-20, General Electric Company (October 1976).
3. D. L. Selby and H. E. Knee, "The 7 and 45 Group CRBR Cross Section Libraries," letter to G. F. Flanagan, May 27, 1977.
4. C. R. Weisbin, R. W. Roussin, J. E. White, and R. Q. Wright, *Specification for Pseudo-Composition-Independent Fine-Group LMFBR Neutron-Gamma Libraries at ORNL*, ORNL/TM-5142 (ENDF-224) Oak Ridge National Laboratory (December 1975).
5. N. C. Paik, et al., *Physics Evaluations and Applications Quarterly Progress Report Ending July 31, 1974*, WARD-XS-3042-7 (July 1974).
6. N. M. Greene, J. L. Lucius, L. M. Petrie, W. E. Ford III, J. E. White, and R. Q. Wright, *AMPX: A Modular Code System for Generating Coupled Multigroup Neutron-Gamma Libraries from ENDF/B*, ORNL/TM-3706 (1976).
7. G. C. Haynes, *The AXMIX Program for Cross Section Mixing and Library Arrangement*, ORNL Central Files Report 74-12-2, Oak Ridge National Laboratory (December 1974).
8. W. A. Rhoades and F. R. Mynatt, *The DOT-III Two Dimensional Discrete Ordinates Transport Code*, ORNL/TM-4280 (September 1973).

9. D. R. Vondy, T. B. Fowler, and G. W. Cunningham, *VENTURE: A Code Block for Solving Multigroup Neutronics Problems Applying to Finite-Difference Diffusion-Theory Approximation to Neutron Transport*, ORNL/TM-5062 (October 1975).

10. D. R. Ferguson, K. L. Derstine, R. C. Borg, and T. A. Daly, "Optimized Iteration Strategies for Fast Reactor Finite-Difference Diffusion-Theory Codes," *Trans. Am. Nuc. Soc.* 22: p. 247 (November 1975).

11. D. R. Ferguson, T. A. Daly, and R. W. Schaefer, *FX2, A Quasistatic Multidimensional Multigroup Diffusion Theory Code with Feedback*, FRA-TM-87, Argonne National Laboratory (April 1976).

12. W. A. Rhoades, *Comments on the DOT 3.5 and DOT 4 Codes.*

13. R. L. Childs, *VIP — A Computer Code Using Two Dimensional Discrete Ordinates Calculations for Cross Section Sensitivity Analysis*, UCCND/CSD-1 (to be published).

14. R. A. Lillie, "Transport Perturbation Code," letter to G. F. Flanagan, (March 17, 1977).

15. E. T. Tomlinson, "Diffusion Theory Perturbation Using DOT Fluxes," letter to G. F. Flanagan (May 3, 1977).

16. *Preliminary Safety Analysis Report for the Clinch River Breeder Reactor Plant*, Project Management Corporation.

17. L. M. Petrie and N. F. Cross, *KENO-IV, An Improved Monte Carlo Criticality Program*, ORNL-4938, Oak Ridge National Laboratory (November 1975).

18. R. L. Childs, Oak Ridge National Laboratory, personal communication, April 1977.

19. J. E. Cahalan, *An Iterative Diffusion Theory Method for the Incorporation of Transport Effects in Fast Reactor Safety Neutronics*, ANL/RAS 76-17, Argonne National Laboratory (May 1976).

20. P. Benoist, "Theories due Coefficient de Diffusion dans un Réseau Compartant des Cavités," Centre d'Etude Nucléaires-Scalay Rep. CEA-R-2278 (1964).

Appendix

A NEW WEIGHTED-DIFFERENCE FORMULATION FOR DISCRETE-ORDINATES CALCULATIONS[1]

One of the shortcomings of the method of discrete ordinates has been a tendency to generate negative estimates of inherently positive fluxes due to over-extrapolation.[2] The complexity of practical transport problems is such that mesh refinement is only a partial remedy. This paper shows a new formulation of an old approach which ensures positive results while retaining satisfactory accuracy.

In the two-dimensional discrete-ordinates transport equation,

$$\mu(A_{i+1}N_{i+1} - A_iN_i) + \eta B(N_{j+1} - N_j) + (\gamma_{m+1}N_{m+1} - \gamma_mN_m) + \sigma NV = SV \ , \tag{1}$$

three of the N's are known from boundary conditions, but assumptions must be made describing the variation of flux across the mesh cell to eliminate three more unknowns. The weighted-difference method for solving Eq. (1) uses three parameters, a, b, and c:[3]

$$N = aN_{i+1} + (1 - a)N_i = bN_{j+1} + (1 - b)N_j = cN_{m+1} + (1 - c)N_m \ . \tag{2}$$

With these,

$$N_{j+1} = \frac{SV + \left(\frac{1-c}{c}\gamma_{m+1} + \gamma_m\right)N_m + \mu\left(\frac{1-a}{a}A_{i+1} + A_i\right)N_i + \left[\eta B - (1-b)\left(\sigma V + \frac{\gamma_m}{c} + \mu\frac{A_{i+1}}{a}\right)\right]N_j}{\sigma V + \frac{\gamma_m}{c} + \eta\frac{B}{b} + \mu\frac{A_{i+1}}{a}} \ . \tag{3}$$

and N_{i+1} and N_{m+1} can be found similarly. When a = b = c = 1/2, Eq. (3) is equivalent to the "diamond-difference" model and assumes a linear variation in flux across the mesh cell. The diamond-difference model provides excellent accuracy for small mesh sizes, and values of a, b, and c < 1/2 are not considered. Unfortunately, the diamond-difference model generates negatives for mesh sizes which are not uncommon in real problems, even though the true result is positive if S is positive. With a = b = c = 1, the "step" model is obtained, equivalent to assuming $N = N_{i+1} = N_{j+1} = N_{m+1}$. This gives inherently positive fluxes, and values of a, b, and c > 1 are not considered.

For many years, a "fix-up strategy" has been used, in which the diamond-difference model is used unless one of the extrapolated fluxes is negative. In that case, all of the fluxes are recalculated using the step model.[4] Another variation involved setting the negative flux to 0 and recalculating the other values.[5] Unfortunately, all fix-up methods can lead to spatial flux distortions and "model-switching" oscillation between iterations, which thwart convergence.

Positivity can also be ensured by adjusting b such that:

$$SV\theta_S + (\gamma_m N_m + \mu A_i N_i)\theta_N + [nB - (1 - b)(\sigma V + 2\mu A_{i+1})]N_j \geq 0 \qquad (4)$$

where θ_S and θ_N are arbitrary multipliers bounded by 0 and 1.

A solution could be found with $\theta_S = \theta_N = 1$, but this can lead to degeneracy in certain cases, producing numbers near 0 which thwart convergence once again. The DOT III code used $\theta_S = 1$ and $\theta_N = \theta$. This provided good results for deep-penetration problems, but failed for criticality calculations due to excessive leakage. Consideration of a difficult reactor cell problem

reveals why this happens. Cell problems typically have tall, narrow space cells. In zones having no source, (4) requires use of the step model along the height of the cell, even though flow across the vertical boundaries would control the actual result of (3) and produce a satisfactory value.

The DOT IV code includes a "θ-weighted" option in which θ_S and θ_N are arbitrarily set to 0.9. This allows the accurate linear model to be used where it is adequate and gives a smooth transition to the step model when the linear model actually breaks down. Either the DOT III or θ-weighted method cost roughly 15% more per iteration than the linear model with step fix-up, but smooth, rapid convergence is found for problems which would otherwise oscillate. Table A1 shows the convergence of a cell problem using the methods described, as well as one where the θ-weighted model is used as a fix-up to the linear model. The requirement for weighted difference in problems of this class is apparent.

Table A2 shows that the θ-weighted model compares favorably with the fix-up models in matching the Monte Carlo result, which is assumed accurate. The new model, then, gives the desired smooth convergence without compromising accuracy.

Table A1. Flux-Convergence Reached Using Various Numerical Models*

Outer Iterations	Linear/ Step	Linear/ Weighted	DOT III Weighted	0- Weighted
1	1.2	1.7	0.3	0.5
2	0.6	0.5	0.1	0.2
3	1.2	1.2	0.7	0.05
4	0.5	0.5	0.03	0.04
5	0.2	0.4	0.03	0.01
6	0.3	0.09	0.01	0.01
7	0.3	0.3	0.006	0.006

*Convergence for the m^{th} inner iteration is defined as:

$$\frac{\phi_m - \phi_{m-1}}{\phi_m}$$

Table A2. Values of K-Effective For a Difficult Cell Problem Using Various Numerical Methods

Example	Code	Energy Groups	Method	K-Effective
1	DOT IV	11	Linear with step fix-up	0.996
2	DOT IV	11	Linear with weighted fix-up	0.996
3	DOT IV	11	DOT III style weighted difference	0.930
4	DOT IV	11	0-weighted difference	0.991
5	DOT IV	51	Li. . with weighted fix-up	0.998
6	MORSE	51	Multigroup Monte Carlo	0.988 ± 0.015

Note (1): K_{eff} was converged to ±0.001 in the DOT cases.

(2): If 0.002 is taken as an "11-group library correction," based on example 5 vs example 2, the 0-weighted result for 51 groups would be 0.993, compared with the MORSE result 0.988 ±0.015.

APPENDIX REFERENCES

(1) W. A. Rhoades and W. W. Engle, Jr., "A New Weighted-Difference Formulation For Discrete-Ordinates Calculations," submitted to ANS Winter Meeting, San Francisco, CA., November 1977.

(2) B. G. Carlson and K. D. Lathrop, "Transport Theory – The Method of Discrete Ordinates," Los Alamos Scientific Laboratory, LA-3251-MS Revised, 1965.

(3) K. D. Lathrop, "Spatial Differencing of the Transport Equation: Positivity vs Accuracy," *J. Comput. Phys.*, 4, 475 (1969).

(4) F. R. Mynatt, et al, "Development of Two-Dimensional Discrete Ordinates Transport Theory for Radiation Shielding," Union Carbide Corporation, CTC/INF-952 (1968).

(5) K. D. Lathrop and F. W. Brinkley, "TWOTRAN-II: An Interfaced, Exportable Version of the TWOTRAN Code for Two-Dimensional Transport," Los Alamos Scientific Laboratory, LA-4848-MS (1973).